Distinct outputs of CDC-42 combine to activate and brake contractility in M-phase *C. elegans* embryos

Authors and order

March 15, 2024

Cell polarity is essential for many aspects of organismal development and physiology, including stem cell dynamics, directional cell migration, and asymmetric cell division [6, 9, 12, 17]. For most cells, the first step in polarization involves a symmetry-breaking response to a transient localized cue that creates asymmetric distributions of specific molecules or molecular activities. The mechanisms that underlie cellular symmetry-breaking have been extensively explored [16], but mechanisms that maintain polarity as a dynamically stable state after the initial polarizing cue is gone have only recently come under scrutiny [25, 11].

On a large scale, a cell's polarity state is encoded by asymmetric distributions of protein molecules, which are shaped by smaller-scale processes like binding, diffusion, and active transport. In *C. elegans*, polarity is encoded by the distribution of two distinct groups of (highly conserved) polarity proteins: anterior PARs (aPARs), which include the scaffold PAR-3, adaptor PAR-6, atypical kinase PKC-3, and GTPase CDC-42, and posterior PARs (pPARs), which include the ring-domain containing protein PAR-2 [1], kinase PAR-1, tumor suppressor LGL-1, and CDC-42 GAP CHIN-1 [15].

Wild-type embryos polarize in two distinct phases termed "establishment" and "maintenance" [5]. In establishment phase, signal(s) from the sperm centrosome/microtubule organizing center (the sperm MTOC) that forms near the site of sperm entry act to load PAR-2 onto the membrane, while at the same time promoting strong anterior-directed actomyosin flows which segregate the PAR proteins into anterior and posterior camps [21, 7]. Near the end of polarity establishment, the centrosomes (and thus the initial polarizing cue) and pronuclei migrate towards the cell center. However complementary PAR domains are stably maintained for approximately 10 minutes between pronuclear meeting and cytokinesis. The PAR proteins act during this interval to promote the asymmetrical enrichment of cytoplasmic cell fate determinants, including P granules, Pie-1 and Mex

proteins [4, 5], and to promote asymmetric distributions of additional cortical factors, including GPR1/2, Let-99, and Lin-5 [24, 29], that control spindle position to ensure the correct partitioning of these determinants into daughter cells during the first asymmetric cleavage (reviewed in [10]).

In the language of dynamical systems, it can therefore be said that the *C. elegans* embryo possesses two stable states: a uniform state, in which all of the proteins are distributed symmetrically throughout the cell, and a polarized state, in which the PAR proteins are sorted into their respective domains. The switch between the two states is then governed by the sperm cue, which drives an advective flow to transform the uniform state to the polarized one [8, 11]. Indeed, recent theoretical and experimental studies showed that the cell operates in a regime where cues are necessary to establish polarity, thus avoiding the potentially chaotic case of spontaneous polarization without cues [11].

This analysis suggests that cue-driven flows are required for polarity establishment. Yet, it has been demonstrated repeatedly that embryos lacking a functional flow during establishment phase still polarize, albeit in a delayed manner, and furthermore find the same boundary position as embryos with a functional establishment-phase flow [31, 28]. The flows in these embryos result from a switch from rho-dependent contractility in establishment phase to CDC-42-dependent contractility in maintenance phase [27], and reveal that maintenance phase biochemistry is designed not just to maintain existing asymmetries, but to find a unique polarized state with a fixed boundary position.

A puzzling feature of the steady state observed in late maintenance phase is an anterior directed flow that results from a persistent contractile asymmetry [25]. In wild type embryos, myosin accumulates at the anterior in a cap that takes up about 50% of the embryo, and myosin flows from the posterior half of the embryo into the anterior cap. Yet despite the flow of myosin and the consequent A/P asymmetry in contractility, the cap maintains a fixed size (it does not contract), and the flow profile in the anterior is roughly zero [25]. This paper sets out to answer the key question posed by these observations: how can the cell maintain a steady state with persistent contractile asymmetries?

Our answer to this question combines experiments and continuum theoretical modeling, and is based on distinct outputs of CDC-42 having different effects on contractility. In the first part of this study, we demonstrate how cell cycle progression (from interphase to mitosis) facilitates a switch from rho-mediated contractility [26, 20, 19] to CDC-42 mediated contractility. The consequences of this switch are non-trivial: because CDC-42 is also an aPAR protein which is inhibited by the pPAR CHIN-1 [25], it couples contractility to the underlying PAR protein circuit.

In the second part of this study, we take a closer look at contractility in maintenance phase. Using a mutant with the dysfunctional RhoGEF ECT-2 [31], we inhibit contractility during establishment phase, thereby allowing polarization to be mediated by CDC-42. Imaging the myosin intensity and flow profile over time reveals an initially fast rescue process, followed by a sharp braking of the boundary and decrease in the flow. The resulting myosin and flow profiles in late maintenance phase agree with the steady state in wild type embryos, which demonstrates that the state we observe is a consequence of *maintenance* phase biochemistry and contractility, and does not require flows in establishment phase.

To understand how the PAR protein circuit (which involves CDC-42) interacts with myosin contractility to maintain a stable polarized state, we introduce a continuum model in the third part of this study. We demonstrate that PAR asymmetries, once set up, can be maintained at a fixed boundary position in the absence of flow. We demonstrate, however, that a model of maintenance phase rescue which is based only on cytoplasmic depletion [8] cannot reproduce the experimental observation of a sudden braking of boundary progression. The model shows that stoppage of boundary progression requires an active decrease in the amount of tension in the anterior over time, until the tension between the anterior and posterior balance.

In the final part of this paper, we use experiments to demonstrate that branched actin in the anterior acts to reduce tension [22, 30] and prevent excessive contraction in the anterior. We repeat our rescue experiments with inhibition of branched actin, and demonstrate a hyper-contractile state where the anterior cap contracts off the end of the embryo. Our model reveals that adding a threshold of CDC-42, at which branched actin is produced, is sufficient to reproduce the initial and latter stages of rescue, with the caveat that additional assumptions about branched actin are required to reproduce all experimental observations.

1 The distinction between establishment and maintenance

Figure we want to make for this section:

(a) ?

(A) Cell cycle progression controls a regime change from rho-dependent contractility to CDC-dependent contractility.

(B) Relaxation of pseudo-cleavage is a marker for this transition (so is onset of centration).

(C) CDC-42 also involved in biochemistry (complexing with PAR-6/PKC-3 to inhibit pPARs), so biochemistry and contractility are intimately coupled in maintenance phase (different from establishment phase where rho has its own pulsatile/oscillatory dynamics).

2 The steady state of maintenance phase

It has been previously observed that embryos in late-maintenance phase exhibit a steady pattern of anterior-directed cortical flow (see [25, Fig. 2]). Yet, despite the anterior-directed contractility, the A/P boundary in late maintenance appears to be stable. It remains unclear if this pattern of flow is a consequence of establishment-phase patterning of myosin [21], or if the pattern of flow is merely transient and would eventually stop if the cell cycle extended long enough. In this section, we establish that the pattern of flow and myosin profile in maintenance phase are in fact robust (to changes in establishment phase contractility) and long-lasting (if maintenance phase is extended); in other words, we seek to show that maintenance-phase biochemistry encodes an attractive steady state.

Figure we want to make for this section:

(a) Kymograph showing rescue
(b) Pictures of myosin distribution in early and late maintenance in wild type and ts ect-2
(c) Fig. 1 in this report (showing progression of myosin and flow over time)
(d) Kymograph from MRCK (RNAi) experiment showing failure of rescue
(e) Kymograph from CDK-1 experiment showing boundary is stable
(f) We will not show messy flows and myosin (from CDK-1) but put those in SI

2.1 Maintenance-phase rescue

In addition to stabilizing asymmetries that are set up during establishment phase, the biochemical and mechanical interactions in maintenance phase can also rescue a steady polarized state. While this has been observed in previous studies in *ect-2* mutants [31, 28], which cannot activate Rho and consequently lack myosin functionality during establishment phase, it has yet to be shown that the steady polarized state that results is the same as in wild-type embryos. To establish this, we systematically image rescue of symmetry breaking in temperature-sensitive *ect-2* mutants, marking the beginning of maintenance phase via the transition of myosin from large to small clusters, and the end of maintenance phase as the onset of embryo rotation prior to cytokinesis. This gives a

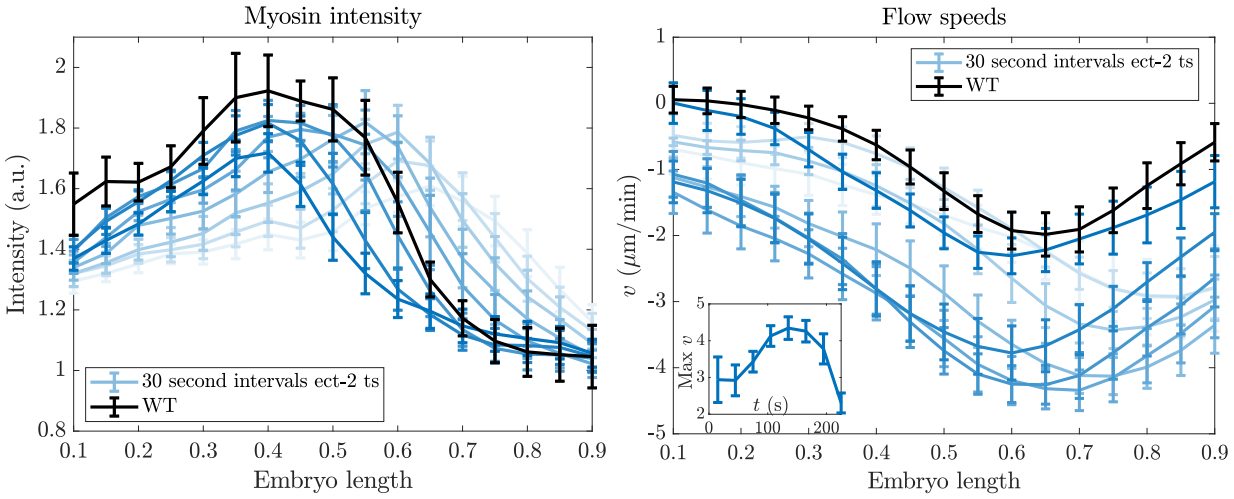

Figure 1: Comparing the end of maintenance phase in *ts ect-2* mutants to wild-type embryos. Left panel: myosin intensity profile. Right panel: flow speeds (inset shows the maximum flow speed over time). The blue colored lines show 30-second intervals of maintenance phase in *ts ect-2* embryos, with darker blue denoting later times. The black line shows the profile extracted from the last minute of maintenance phase in wild type embryos [25].

roughly four minute window of maintenance phase for each embryo, in which we track the average myosin intensity profile and flow speed.

In Fig. 1 we show the myosin intensity and flow speed over 30 second intervals of maintenance phase rescue, and compare the result to the steady myosin intensities and flow speeds observed in wild-type embryos [25]. The myosin peak initially grows in size advances rapidly towards the anterior, but after about three minutes it stops growing and becomes pinned at about 40% embryo length. The pinning of the myosin peak corresponds to a decrease in the maximum flow speed from about 4.5 μm/min (from 2:00 to 3:30) to 2 μm/min in the last 30 seconds of maintenance phase (3:30 to 4:00, see the inset of Fig. 1). In the last 30 seconds of maintenance phase, the flow profile in *ts ect-2* embryos is roughly the same as that observed during late maintenance phase in wild-type embryos. The myosin intensity appears quantitatively different, but has the same fundamental shape: there is a gradient of myosin in both the anterior and posterior, with a maximum occurring at around 40% of the embryo length. These results establish that the biochemical circuit governing maintenance phase can amplify small residual asymmetries from establishment phase, and that the resulting polarized state is independent of what comes before maintenance.

2.1.1 Rescue requires MRCK

Need to show that it cannot happen without myosin flows.

2.2 Extending maintenance phase establishes

The pinning of the myosin boundary and subsequent decrease in the speed of flow hint that the cell has a built-in mechanism to prevent the boundary from contracting off the end of the embryo. But is it really possible to maintain a steady myosin intensity profile in the presence of a persistently anterior-directed flow?

To probe whether the myosin intensity and patterns of flow we see in late maintenance phase are truly steady states, we extend maintenance phase by treating wild-type embryos with CDK-1 (RNAi). Marking the start of maintenance phase by the end of pseudo-cleavage, and the end of maintenance phase by the onset of cytokinesis, we obtain a window of roughly 8–10 minutes per cell, in which we characterize the myosin intensity and flow speeds (see SI). Later stages of the extended maintenance show a relatively stable position of the myosin boundary (it in fact expands towards the posterior slightly) and a persistent anterior-directed flow which tends to achieve a maximum (magnitude) just posterior of the peak myosin location. Because the myosin intensity and flow speeds in *CDK-1* (RNAi) never resemble those of wild-type, it is clear that interfering with CDK-1 affects more than just the cell cycle, and it is impossible to say concretely that the specific flow and myosin profiles in late maintenance are "steady." Nevertheless, we can say definitively that a persistent anterior-directed flow does *not* lead to further contraction of the boundary when maintenance is extended.

3 Model reveals existing mechanisms cannot explain rescue

Our goal in this section is to explore existing literature mechanisms for how maintenance phase biochemistry could set an attractive steady state. At first glance, it appears that the phenomenon of maintenance phase rescue is a consequence of an instability of the underlying system; a small perturbation in the myosin concentration could induce an anterior-directed flow, which drives the system to the polarized state. Here we systematically exclude this by considering a model of myosin alone and showing that spontaneous symmetry breaking is not possible with realistic parameters. We then consider PAR proteins, showing that, while the PAR circuit we consider can maintain a stable polarized state with a fixed boundary position, the time required to set up this state is prohibitively long, and myosin-directed flows are required. Finally, we consider a combination of

myosin-driven flows *and* PAR proteins. This model allows us to reproduce the initial stages of maintenance phase rescue, but it cannot explain the sudden slow-down in flow speeds and pinning of the myosin boundary.

Figure we want to make for this section:

(a) Stability analysis for myosin (Fig. 2 here)
(b) Schematic of biochemistry model (Fig. 3 here)
(c) Cytoplasmic depletion with PARs (Fig. 4 here)
(d) Attempt at rescue with myosin (Fig. 5 here)

3.1 Myosin without additional feedback cannot spontaneously polarize

We first explore the dynamics of myosin alone, which we describe in terms of a one-dimensional spatially and temporally varying field $M(x,t)$ which evolves according to the advection-diffusion-reaction equations [2]

$$\partial_t M + \partial_x (vM) = D_M \partial_x^2 M + k_M^{\text{on}} M_{\text{cyto}} - k_M^{\text{off}} M \tag{1a}$$

$$\gamma v = \eta \partial_x^2 v + \partial_x \sigma_a(M) \tag{1b}$$

The velocity field (1b) comes from the assumption that myosin generates an active stress $\sigma_a(M)$, which combines with the viscous stress to give the total cortical stress $\sigma = \eta \partial_x v + \sigma_a(M)$. The force balance equation in the fluid says that the force due to stress must be balanced by the drag force, $\gamma v = \partial_x \sigma$, where γ is the drag coefficient. Combining the force balance with the stress expression gives the velocity equation (1b), which can also be rewritten in terms of the "hydrodynamic lengthscale" $\ell = \sqrt{\eta/\gamma} \approx 14$ μm, which is essentially the lengthscale on which a local increase in the myosin field will pull in neighboring molecules [18]. As in [2], we ignore the elastic part of the stress, since the actomyosin cortex is purely viscous on timescales longer than the cortical turnover time [18].

In the case when diffusion of myosin is negligible and all myosin is bound to the membrane, the stability analysis in the SI shows that the dynamics are unstable when the flow carries myosin molecules a distance larger than the hydrodynamic lengthscale, i.e., $v/k_M^{\text{off}} > \ell$. Substituting $\ell \approx 14$ μm, we plot the velocity threshold for instability as a function of myosin lifetime in Fig. 2. For realistic lifetimes on the order 5–20 s, the minimum flow speed to generate instability is about 40 μm/min, which is much faster than ever observed *in vivo*. Thus the dynamics of maintenance phase rescue are not due to myosin instabilities.[1]

[1] We note a distinction here between maintenance and establishment phase. In the latter, instabilities in the

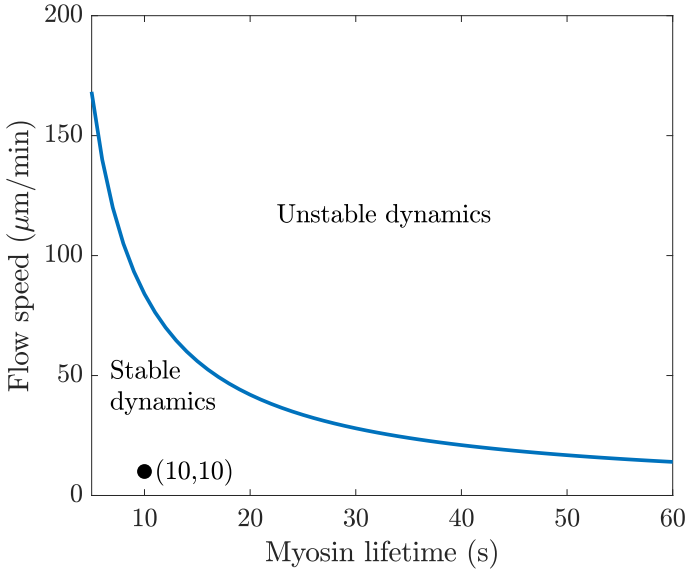

Figure 2: Required flow speeds for spontaneous polarization of myosin during maintenance phase. We plot $v = \ell/\tau_M$, where $\tau_m = 1/k_M^{\text{off}}$ is the myosin lifetime and $\ell = 14$ μm is the hydrodynamic lengthscale. Flow speeds above the blue line give unstable dynamics, while flow speeds below it give stable dynamics.

3.2 Basic maintenance-phase biochemistry circuit

Because the dynamics of myosin alone are insufficient to generate instability, PAR proteins must be essential for rescue to occur [31]. We consequently introduce a model of maintenance phase biochemistry based on the diagram in Fig. 3, which in turn comes from [15, Fig. 2]. On the anterior side, we have three distinct protein species: PAR-3 (A), CDC-42 (C), and PAR-6/PKC-3 (K), each of which has a separate function. The posterior PARs (PAR-2, PAR-1, and CHIN-1) can be lumped into one species (denoted by P), which antagonizes both PAR-3 and CDC-42. The dimensional equations which describe the circuit are

$$\begin{aligned}\partial_t A_1 = {} & D_A \partial_x^2 A_1 + \left(k_A^{\text{on}} + k_A^+ f_A^+(A)\right) A_{\text{cyto}} - k_A^{\text{off}} A_1 \\ & + 2k_A^{\text{dp}}(P)\hat{A}_2 - 2k_A^{\text{p}} \hat{A_1}^2 + \sum_{n=3}^{N} \left(A_n - k_A^{\text{dp}}(P) A_1 A_{n-1}\right)\end{aligned} \tag{2a}$$

$$\partial_t A_n = k_A^{\text{p}} A_1 (A_{n-1} - A_n) - k_A^{\text{dp}}(P)(A_n - A_{n+1}) \qquad N > n \geq 2 \tag{2b}$$

$$\partial_t A_N = k_A^{\text{p}} A_1 A_{N-1} - k_A^{\text{dp}}(P) A_N \tag{2c}$$

dynamics of rho combine with delayed negative feedback to yield pulsatile dynamics [23, 20, 19]. The connection between these pulsatile dynamics and the large-scale flows that establish polarity is still unknown.

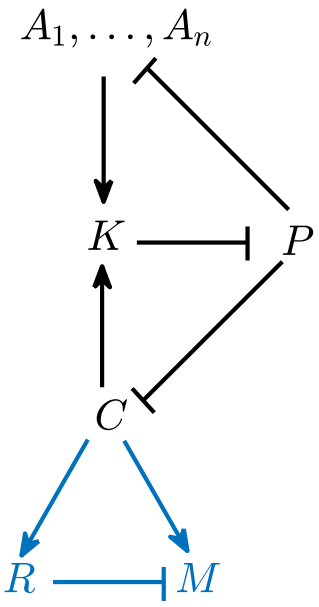

Figure 3: Schematic of the biochemistry model. We consider the black parts (biochemistry only) in Section 3.2, and add the blue parts (contractility) in Section 3.3. On the anterior half, A represents PAR-3 (in monomer and oligomer form), K represents the PAR-6/PKC-3 complex, and C represents CDC-42. The posterior PARs can be represented by a single protein species P.

$$\partial_t C = D_C \partial_x^2 C + k_C^{\text{on}} C_{\text{cyto}} - k_C^{\text{off}} \left(1 + r_{\text{PC}} P\right) C \tag{2d}$$

$$\partial_t K = D_K \partial_x^2 K + r_{\text{ACK}} C \delta_{A>A_0} K_{\text{cyto}} - k_K^{\text{off}} K \tag{2e}$$

$$\partial_t P = D_P \partial_x^2 P + k_P^{\text{on}} P_{\text{cyto}} - k_P^{\text{off}} \left(1 + r_{\text{KP}} K\right) P \tag{2f}$$

The PAR-3 equations (2a)–(2c) describe the dynamics of PAR-3 oligomerization (an oligomer of size n denoted by A_n), for which we use the model developed in [14]. As discussed in detail there, the combination of oligomerization and positive feedback (through the term $k_A^+ f_A^+(A)$) imparts intrinsic bistability to the system. This bistability is strengthened when pPARs are included; through the term $k_A^{\text{dp}}(P)$, these posterior PARs promote depolymerization of PAR-3.

PAR-3 also gates the association of CDC-42 with PAR-6/PKC-3 (K), which is a complex that inhibits all posterior PARs [15]. To model this, we work off the observations in [25], which reveal that PAR-6/PKC-3 are recruited to the membrane by CDC-42, provided that there is a sufficient concentration (roughly 10% of the enriched anterior level) of PAR-3 on the membrane. Thus the total loading term in (2e) is proportional to the CDC-42 concentration times the cytoplasmic concentration of K, provided the PAR-3 concentration satisfies $A > A_0$. The other two equations (for CDC-42 and pPARs) are straightforward: we assume a basal rate of binding and unbinding,

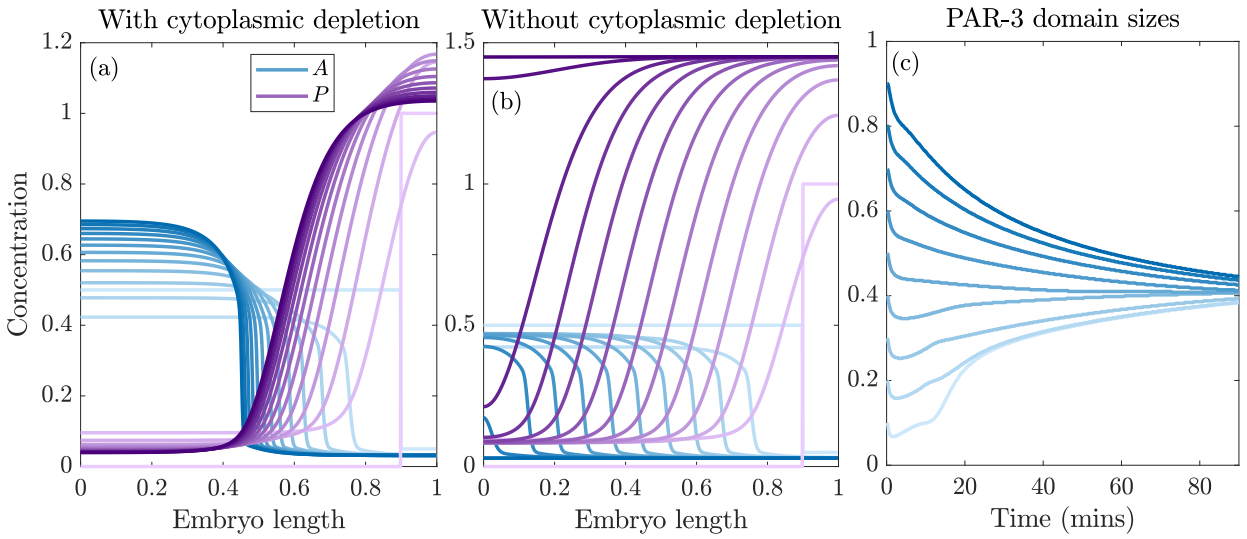

Figure 4: The biochemistry model (2) has a unique boundary position controlled by cytoplasmic depletion, which can only be achieved in realistic timescales if started near the equilibrium position. We simulate the progression of initially separated aPAR/pPAR domains. (a) 90% initial PAR-3 domain size with cytoplasmic depletion. (b) 90% initial PAR-3 domain size *without* cytoplasmic depletion after $t = 10$ mins. A sequence of 13 time points from $t = 0$ (lightest colors) to $t = 120$ mins (darkest colors) is shown. (c) PAR-3 domain size (length where the PAR-3 concentration is 80% of the maximum or larger) over time starting from varied initial conditions.

with an unbinding rate which is linearly enhanced by the inhibitor (pPARs for CDC-42 and PKC-3 for pPARs). In the supplemental appendix, we nondimensionalize (2), then use sets of existing experimental observations about the relative amount of each species on the anterior/posterior side of the embryo, as well as estimates of the amounts in the cortex vs. cytoplasm, to constrain the unknown parameters.

3.2.1 PAR proteins without contractility amplify asymmetries, but too slowly

In previous work on PAR-3 [14], we demonstrated that the diffusion of the smaller oligomer sizes (monomers in our model) sets a unique boundary position. In Fig. 4, we demonstrate that this with the full biochemistry by simulating the contraction of a PAR-3 domain that initially takes up 90% of the embryo. The boundary shifts because a high concentration of pPARs shifts the local equilibrium of PAR-3 oligomerization towards the monomer state, which makes bistability impossible [14]. Consequently, we observe contraction of the PAR-3 domain, with a peak that grows over time, and expansion of the PAR-2 domain, both of which eventually reach a steady

state. The concentration of PAR-2 at the edge of the domain decreases over time, which suggests that cytoplasmic depletion might be responsible for pinning the boundary. To demonstrate that a fixed pool of protein is key to arresting posterior domain expansion, in the right panel of Fig. 4 we simulate with a cytoplasmic pool that is "frozen" at its value at $t = 10$ mins. The result is an anterior domain which shrinks at a constant rate with constant peak concentration, and a posterior domain which expands at a constant rate with the same concentration at the edge. Given enough time, the posterior domain invades the entire embryo length.

In [14], we showed that the diffusion-controlled shift of the PAR-3 boundary occurs on timescales of hours, meaning that the boundary never reaches a steady position in practice. This is confirmed in Fig. 4, which shows that cytoplasmic depletion can only act rapidly to stop boundary progression if the initial boundary size is close to the steady state. The simulation in Fig. 4(a), which starts at 90% PAR-3 enrichment takes some two hours to reach the steady state; while a simulation starting at 50% PAR-3 enrichment takes only 5–10 minutes. In order to reproduce rescue, we need to introduce cortical flows that initially shift the boundary at a faster initial rate. If these cortial flows are then arrested, cytoplasmic depletion can then prevent the boundary from shifting, leading to a steady state.

3.3 Coupling contractility to biochemistry reproduces initial stages of rescue

Because neither myosins nor PAR proteins can rescue maintenance phase asymmetries by themselves, there must be an interaction with PAR proteins that amplifies gradients in contractility to rescue the correct polarized state. To account for this, we add the myosin dynamics (1) to the biochemistry system (2). In doing this, we also incorporate advective terms that ensure that each protein moves with the local cortical velocity [13], and make CDC-42 a promoter of myosin. The equations corresponding to this situation are a straightforward extension of (1) and (2), and we therefore confine them to the supplemental material, where we give a non-dimensional version and fit the unknown parameters.

In Figure 5 shows the results when we the parameters to match the experimentally-measured initial speeds of rescue. The left panel shows the dynamics of the simulation from $t = 0$ (lightest colors) to $t = 7.5$ mins (darkest colors), while the right panel shows the myosin boundary position (0 is the anterior pole, 1 is the posterior pole) and the flow speeds over time. Our statistics show the beginning of the rescue process, where an initially peaked profile of PAR-2 invades the anterior domain, concentrating anterior PARs in the middle and thereby increasing the concentration of

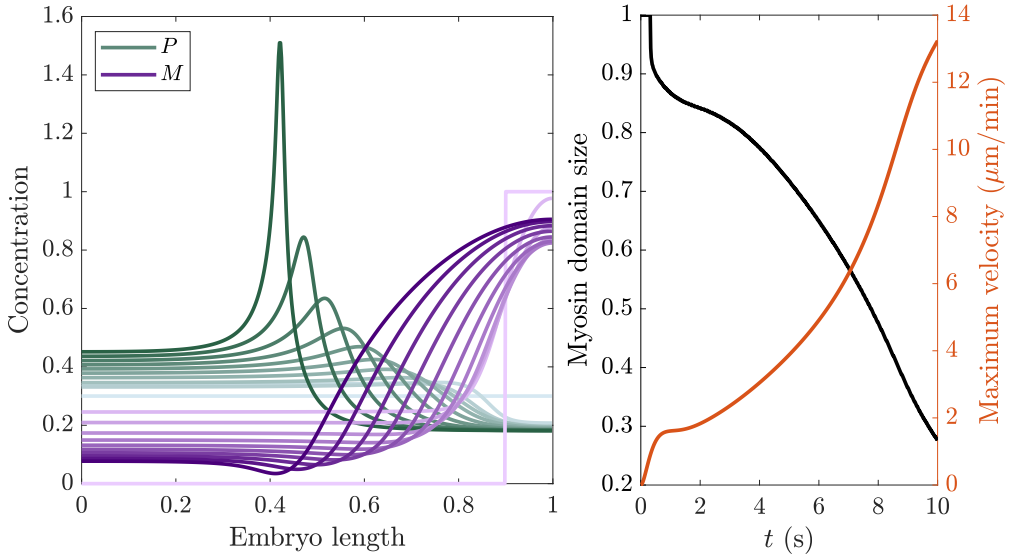

Figure 5: Simulating rescue with a coupled model of contractility and biochemistry. Left panel: time course of rescue, with lines shown at equal time points from $t = 0$ to $t = 7.5$ mins (intervals of 45 seconds). The green and purple lines show pPARs (P) and myosin (M), respectively. Right panel: the myosin domain size (proportion of the domain with concentration > 0.25) over time (black curve, left axis) and the corresponding flow speed (red curve, right axis).

pPARs in the posterior. As a result of this, CDC-42 gets inhibited in the posterior, which gives a gradient of myosin from posterior to anterior. The gradient of myosin generates a flow which further compacts the anterior domain. The timescale of this compaction is much faster than without flows (Fig. 4), and indeed occurs on a timescale of minutes and not hours.

While our model reproduces the initial stages of the rescue process, there is no mechanism in it to halt the advancing myosin front. With the correct model parameters, the tendency of flow to concentrate the aPARs overwhelms the effect of cytoplasmic depletion (which tends to slow the boundary motion). As a result, the boundary contracts with nothing to slow it down. Indeed, in the limit as time goes to infinity, we expect one peak of aPARs and myosin at the anterior pole, which is in sharp contrast to our experimental result which showed a sharp drop in the anterior-directed flow speed in the late stages of maintenance phase (see inset of Fig. 1).

4 Branched actin as a brake on contractility

Our modeling so far identified two regimes of behavior, depending on the sensitivity of myosin to the CDC-42 concentration. Roughly speaking, if CDC-42 promotes myosin at a rate much smaller than the basal rate (0 in Fig. 4), the cytoplasmic dynamics are sufficient to stop the pPARs from invading too far into the anterior domain. But this model has to be discarded because the dynamics occur over unrealistically long timescales. To match the speed of rescue, CDC-42 has to promote myosin at a rate much larger than the basal rate, which leads to fast flows and (in this model) a rapid concentration of the anterior domain into a peaked profile at the anterior pole (Fig. 5). Thus, we are missing an important interaction that slows down the advancing myosin peak, rapidly dropping the flow speed and allowing cytoplasmic depletion to pin the boundary. This interaction is the focus of this section.

4.1 Experiments in arx-2 (RNAi) embryos establish a hyper-contractile state

Figure we want to make for this section:

(a) Pictures of wild-type vs. *arx-2* (RNAi) embryos in late maintenance
(b) Pictures of ect-2 (ts) with and without arx-2 (RNAi) in early and late maintenance
(c) Kymograph of rescue with and without arx-2 (RNAi)
(d) Whatever quantitative information we can get about myosin intensity and flows

We hypothesize that branched actin might stop the anterior cap from becoming hyper-contractile. To test this hypothesis, we deplete wild type embryos of arx-2, a protein which activates the arp 2/3 complex and the assembly of branched actin. Figure 6 shows the average myosin intensity and flow profiles over the last three minutes of maintenance phase in wild-type (red) and arx-2 (RNAi) treated embryos (blue). While the wild-type intensity seems to be roughly stalled at a boundary position 40% of the embryo length, the arx-2 (RNAi) embryos demonstrate hyper-contractility, with a myosin intensity that only grows in time near the anterior boundary.

The flow measurements in *arx-2* (RNAi) embryos are chaotic and noisy because the hyper-contractile anterior cap is not always positioned directly on the anterior pole, so flows can be generated off the A/P axis. In Fig. 6, we show the average flow speeds in embryos where the A/P flow dominates other directions (6 of the 12 embryos). These flows have a maximum speed around 2.5–4 μm/min. Unlike the wild-type profile, whose point of maximum flow and stall point are roughly constant in time, the *arx-2* (RNAi) flow profiles show no stall point, and have a point of maximum flow which shifts towards the anterior in time. Thus the hyper-contractile state observed

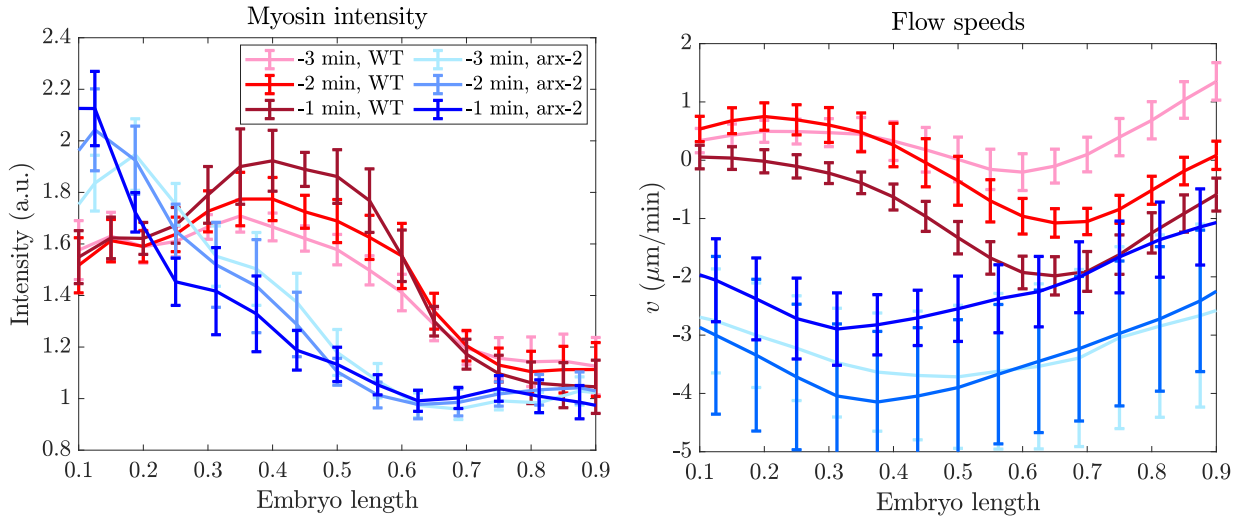

Figure 6: Comparing late maintenance phase in wild-type (red lines) and arx-2 (RNAi) treated embryos (blue lines). The lightest colors show the average profile between 2 and 3 minutes prior to cytokinesis onset, the middle colors between 1 and 2 minutes, and the darkest colors show the profile in the last minute of maintenance phase. Left plot: the myosin intensity profile ($n = 12$ for *arx-2*). Right plot: flow speeds ($n = 6$ for *arx-2*, discarding embryos that do not have A/P axis flows).

in embryos *without* branched actin matches qualitatively matches what our previous model might predicted (a hyper-contractile state). In other words, it is the lack of branched actin inhibiting contractility in our model that makes it fail to reproduce the correct rescue dynamics.

4.2 Model of branched actin

Figure we want to make for this section:

(a) Schematic showing ways we consider branched actin working
(b) Simulation with tension reduction showing boundary stops
(c) "Best" simulation reproducing all trends

To model branched actin, we work off the following two important observations from our maintenance-phase rescue experiments:

1. The pinning of the myosin domain and drop in velocity happen quite abruptly (Fig. 1).

2. The rapid drop in velocity is *not* accompanied by strong changes in the myosin concentration profile (Fig. 1).

These observations together suggest that there is an ultra-sensitive dependence of contractility (not myosin concentration) on branched actin. As rescue progresses, branched actin becomes

concentrated on the anterior, locally becoming more dense, and activating the braking process.

To incorporate branched actin into our modeling framework, we make the following assumptions

1. There exists a threshold of CDC-42 above which branched actin is created. The threshold is reached roughly when the A/P boundary reaches the middle of the cell.

2. Branched actin assembly is autocatalytic, since new branches become sites for additional branches.

3. Branched actin unbinds from the cortex with characteristic rate k_R^{off}.

4. While branched actin does not diffuse in the cortex, polymerization of actin leads to a spreading out of the branched network, and so we include nonzero diffusivity.

Combining these assumptions leads to the advection-diffusion-reaction equation

$$\partial_t R + \partial_x(vR) = D_R \partial_x^2 R + \left(r_{\text{CR}} \max\left(C - C_R, 0\right) + r_{\text{RR}} R\right) R_{\text{cyto}} - k_R^{\text{off}} R \tag{3}$$

for the evolution of branched actin (R) in time and space.

We first assume that branched actin inhibits contractile tension according to the relationship

$$\sigma_a = \frac{\sigma_0 M}{1 + r_{\text{R}\sigma} R}. \tag{4}$$

We use division of the stress instead of subtraction because, as the branched actin concentration goes to infinity, we expect the tension to approach zero, as was shown to be the case *in vitro* using laser ablation [22]. In our model, negative stress corresponds to an expansive force, which has never been seen experimentally.

The dynamics of rescue in this case are shown in Fig. 7. In the early stages of rescue, we see a concentration of myosin and CDC-42 into an interior peak which grows over time. Once the concentration of CDC-42 at the peak exceeds the threshold $C_R = 0.25$, branched actin is produced. This causes an immediate drop in contractility within the peak (see the active stress profile at intermediate times), which leads to a leveling out of the anterior profiles of CDC-42 and myosin (weaker flows in the anterior allow CDC-42 to diffuse over). Following this, branched actin builds up on the anterior. The boundary stops moving when the tension on the anterior balances the tension on the posterior, leaving an intermediate zone of contractility at around 60% embryo length.

While these simulations qualitatively reproduce what we observe in maintenance phase rescue (the anterior boundary progresses and then stops), there are two details that do not match the

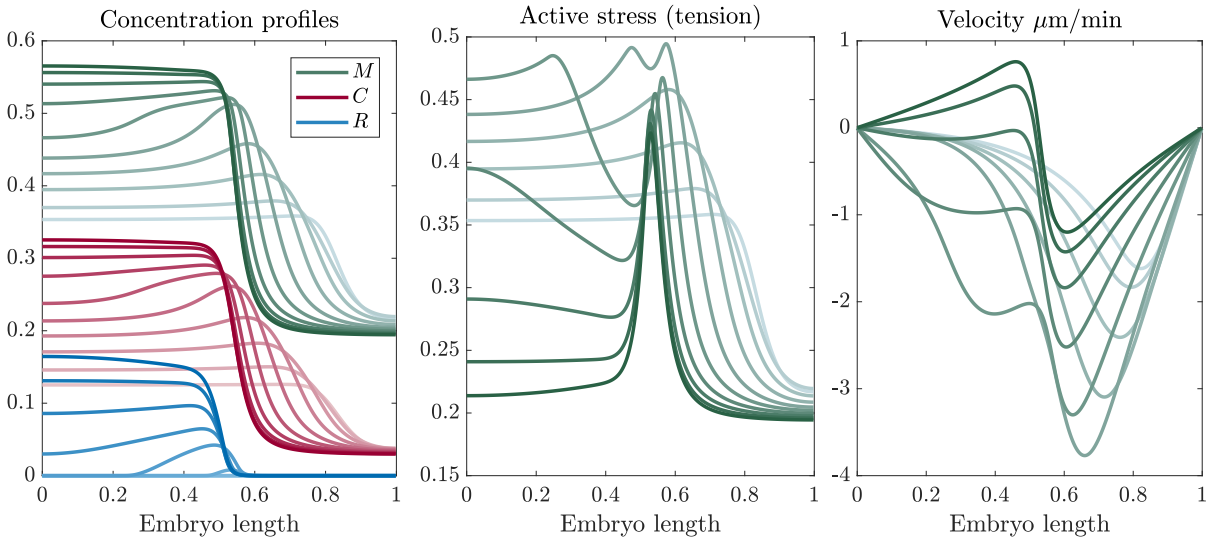

Figure 7: Dynamics of rescue when branched actin inhibits stress/tension according to (4). The left panel shows the concentration profile of myosin (M, green), CDC-42 (C, red), and branched actin (R, blue) over time. The middle panel shows the active stress (tension), normalized by σ_0, and the right panel shows the velocity in units of μm/min. Each panel has a series of ten lines which show the profile at $t = 1, 2, \ldots 10$ min, with darker lines showing later times.

experiments. First, as soon as branched actin inhibits contractility, the myosin concentration profile tends to flatten out in the anterior (it is no longer peaked). This is not what we see in the rescue experiments (data in Fig. 1), where myosin stays peaked after the boundary stops moving. Second, the flow profile from simulations is symmetric about the myosin peak with a flow of about 1 μm/min coming from *both* the anterior and posterior into the zone of contractility. This is also not what we observe in experiments, where the flow profile is essentially flat in the anterior (up to 40% embryo length), and anterior-directed in the posterior (see Fig. 1). In the following sections, we add to our model to try to address these two issues.

4.2.1 Detail 1: reproducing the myosin profile

Let us consider first the issue of the myosin concentration profile. What is missing from our inhibition model that causes myosin to be flat in the anterior? We previously saw that inhibition of tension by branched actin inhibits flows in the anterior, which allows diffusion to level out the anterior CDC-42 profile, which in turn levels out the anterior myosin profile. At steady state, there is a compressive flow in the middle of the embryo, but the speed of the flow (at most 2 μm/min as measured in experiments) is insufficient to concentrate myosin or CDC-42. If flow is insufficient to

concentrate myosin, there must be direct inhibition near the anterior pole.

We propose that, in addition to affecting contractility, branched actin could also inhibit myosin directly in the anterior, for example by thickening the cortex and forcing myosin unbinding (which was shown to occur in mouse oocytes [3]). To implement this in simulations, we modify the myosin equation (**??**) to add the additional term $-r_{\mathrm{RM}}RM$. Figure 8(a) shows the resulting dynamics of rescue when we add this new assumption to our simulation from Fig. 7. As before, the myosin and CDC-42 boundary shifts towards the anterior, until CDC-42 exceeds the critical concentration for branched actin. This time, however, branched actin inhibits myosin, which maintains the peak in myosin that initially occurs from flow. The inhibition of myosin, combined with the reduction of tension, actually lead to an imbalance where the boundary post-rescue shifts back towards the posterior, something that we have observed in embryos with extended maintenance phase. The peak in myosin in this case occurs because branched actin is enriched on a smaller domain than myosin, which leaves a medial zone of contractility where myosin is enriched but branched actin is not.

The inhibition of myosin by branched actin is one way to explain how myosin, which has residence time of about 8 seconds on the cortex, could have an interior peak in its concentration profile, while CDC-42, which has a much longer residence time (and can be advected by the flow for longer) has no such peak (Alex check). An alternative hypothesis is that myosin has a longer residence time on the cortex, as clusters of myosin can be much longer lived than individual molecules. To check this hypothesis, in Fig. 8(b) we show results of simulations where myosin has a residence time of 25 s instead of 8 s, and there is no longer direct inhibition of myosin by branched actin. Unlike CDC-42, which diffuses in the membrane, in our model there is no diffusivity of myosin, so the longer residence time combines with the existing flows to transport myosin into a peak near 60% embryo length. The peak in this case occurs because of advection of myosin into the zone of contractility.

While both models show a better fit to the data as far as the myosin profile, neither have a velocity which matches that obtained from experiments, as there is still a backflow in the anterior which results from the reduction of tension and myosin inhibition.

4.2.2 Detail 2: reproducing the (lack of) flow on the anterior

Experiments make clear that the tension profile in the anterior is lower than in the contractile midzone. There is already an enrichment of myosin at the midline relative to the anterior pole, which

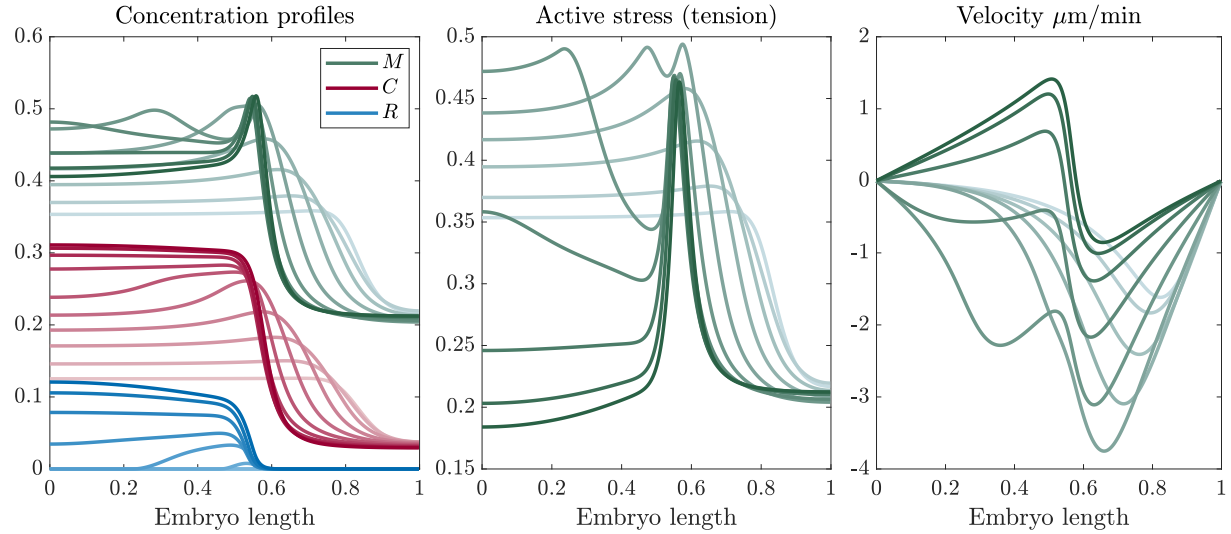

(a) Direct inhibition of myosin by branched actin ($\hat{R}_{\mathrm{RM}} = 2$)

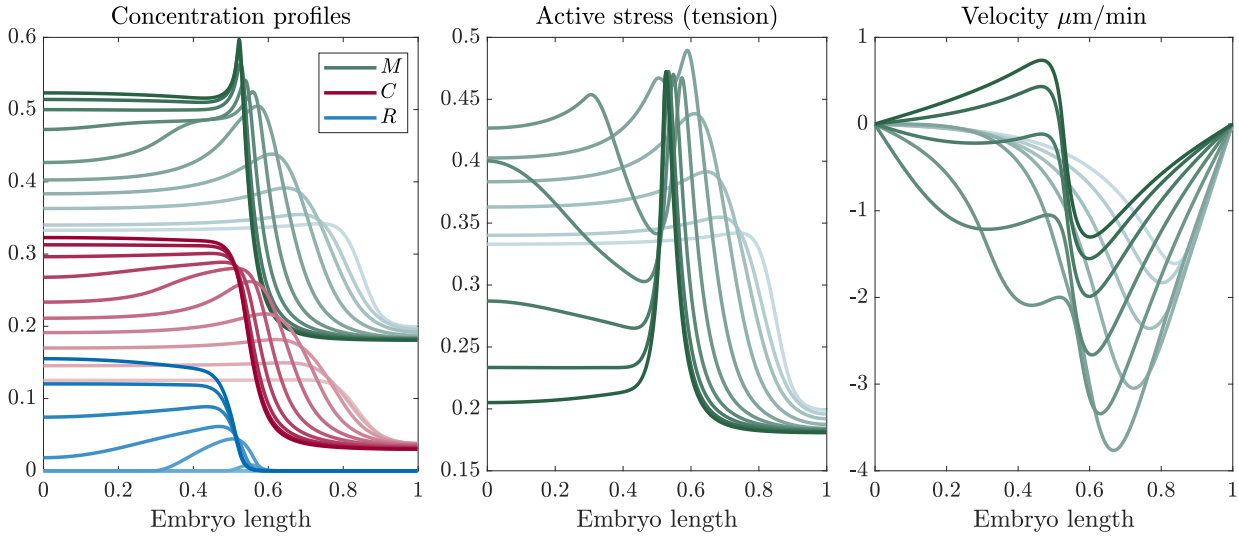

(b) Longer myosin lifetime (25 s)

Figure 8: Two models for how an interior peak of myosin could be maintained. (a) Branched actin directly inhibits myosin in addition to inhibiting stress. (b) The myosin lifetime increases (globally) from 8 s to 25 s. The left panel shows the concentration profile of myosin (M, green), CDC-42 (C, red), and branched actin (R, blue) over time. The middle panel shows the active stress (tension), normalized by σ_0, and the right panel shows the velocity in units of μm/min. Each panel has a series of ten lines which show the profile at $t = 1, 2, \ldots 10$ min, with darker lines showing later times.

should give a gradient in tension and induce a flow towards the midline. Our simulations have demonstrated that this gradient not only exists, but is accentuated by branched actin's inhibition of tension, which is necessary to stop the boundary from progressing.

How is it, then, that there is no flow from the anterior pole towards the anterior cap? In wild-type and *ect-2* (ts) embryos in late maintenance, we never detect a substantial (larger than 1 μm/min) backflow in the anterior (see Fig. 1), despite the gradient in myosin (and presumably tension). Put another way, gradients in tension do not translate to flows the same way in the anterior as they do in the posterior, presumably because of gradients in branched actin.

Our model equation for velocity (1b) has two addition parameters that model how flow responds to changes in contractility. The parameter that controls the magnitude of the flow obtained for a fixed tension gradient is the drag or friction coefficient γ, and the parameter that controls the response to a given rate of strain ($\partial_x v$) is η. We propose that branched actin could modulate each of these parameters according to the linear relationships

$$\gamma(R) = 1 + r_{\mathrm{R}\gamma} R \qquad \eta(R) = 1 + r_{\mathrm{R}\eta} R.$$

These two models, while superficially similar, are at a deeper level quite different. In the case of increased friction, we are proposing that the velocity can rapidly change from negative (in the posterior) to positive (in the anterior), but that the magnitude of the positive velocity in the anterior is necessarily smaller because the same force on that side generates a smaller velocity than on the posterior. Increased viscosity, by contrast, says that the branched actin network resists changes in strain rate (sharp changes in velocity). By increasing viscosity, we are proposing that the changes in tension on the anterior side cannot induce compressive flows because of viscous resistance.

Starting from the simulations in Fig. 8(b) (which have increased myosin lifetime to generate a myosin peak), we consider moderate changes in friction/viscosity with branched actin, choosing parameters to roughly double the friction/viscosity on the anterior relative to the posterior. In Fig. 9, we plot the resulting dynamics of rescue. Both simulations show a maximum in the flow intensity, followed by a gradual decrease in the flow speeds to a steady profile. The simulations with larger viscosity have a flow profile which is smoother (by design), and hence agrees more with experiments, but they tend to smooth the myosin cap so that it becomes almost non-existent. Simulations with increased friction do not show this, but they still retain a small compressive flow in the anterior. The simple fact is that the experimental flow profile (no compression from the anterior) does not concentrate myosin, even with the longer residence time.

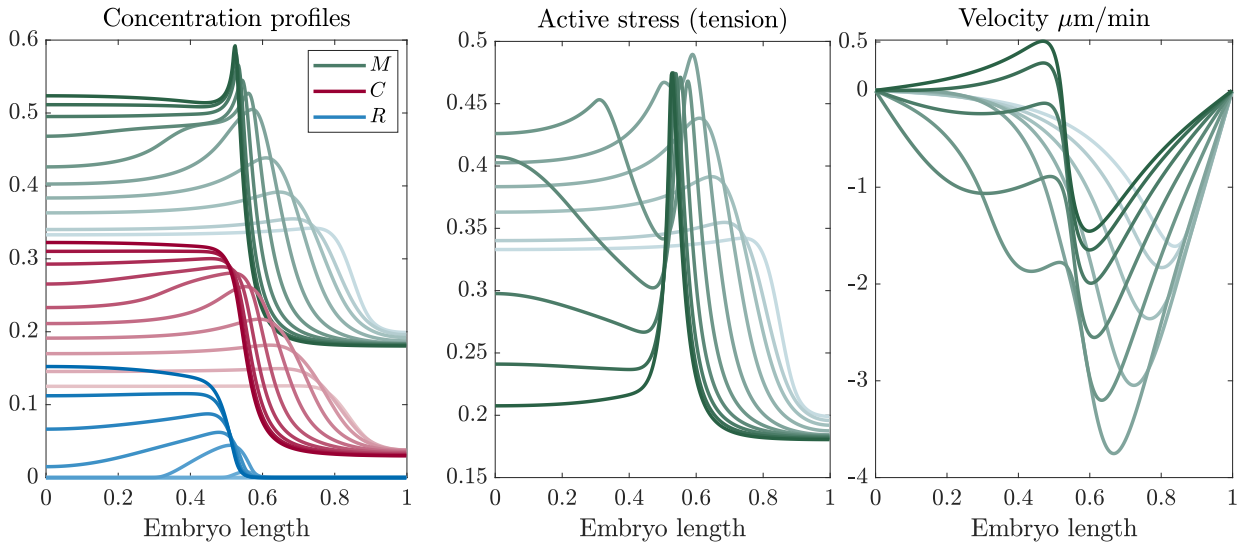

(a) Increased friction ($r_{\mathrm{R}\gamma} = 10$)

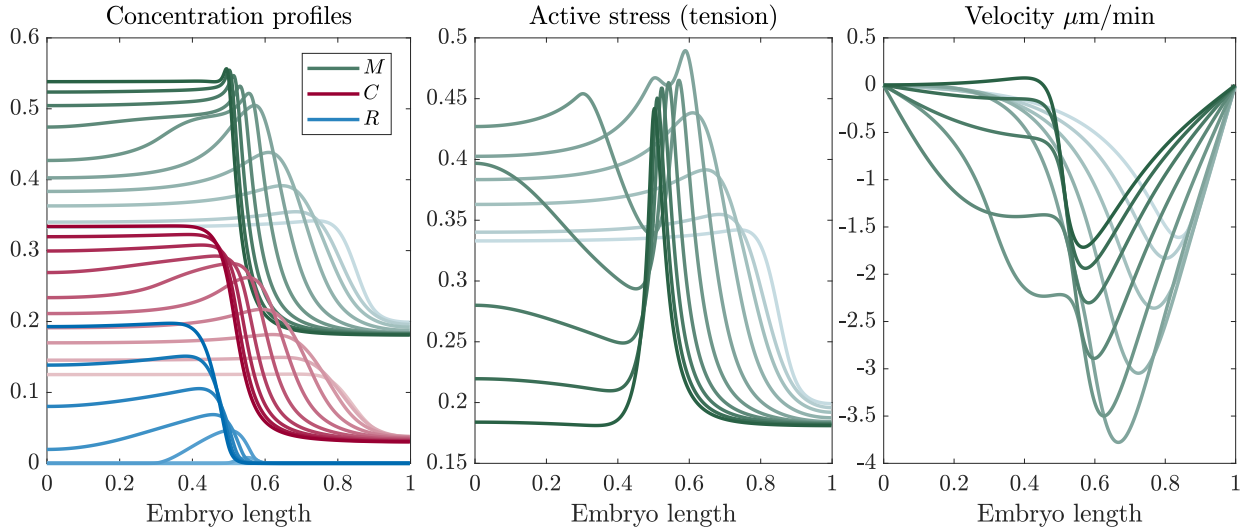

(b) Increased viscosity ($r_{\mathrm{R}\eta} = 5$)

Figure 9: Dynamics of rescue when branched actin has *mild* effects on the response to stress. In (a) viscosity is constant and friction increases according to $\gamma(R) = 1 + r_{\mathrm{R}\gamma}R$, while in (b) friction is constant and viscosity increases according to $\eta(R) = 1 + r_{\mathrm{R}\eta}R$. The left panel shows the concentration profile of myosin (M, green), CDC-42 (C, red), and branched actin (R, blue) over time. The middle panel shows the active stress (tension), normalized by σ_0, and the right panel shows the velocity in units of μm/min. Each panel has a series of ten lines which show the profile at $t = 1, 2, \ldots 10$ min, with darker lines showing later times.

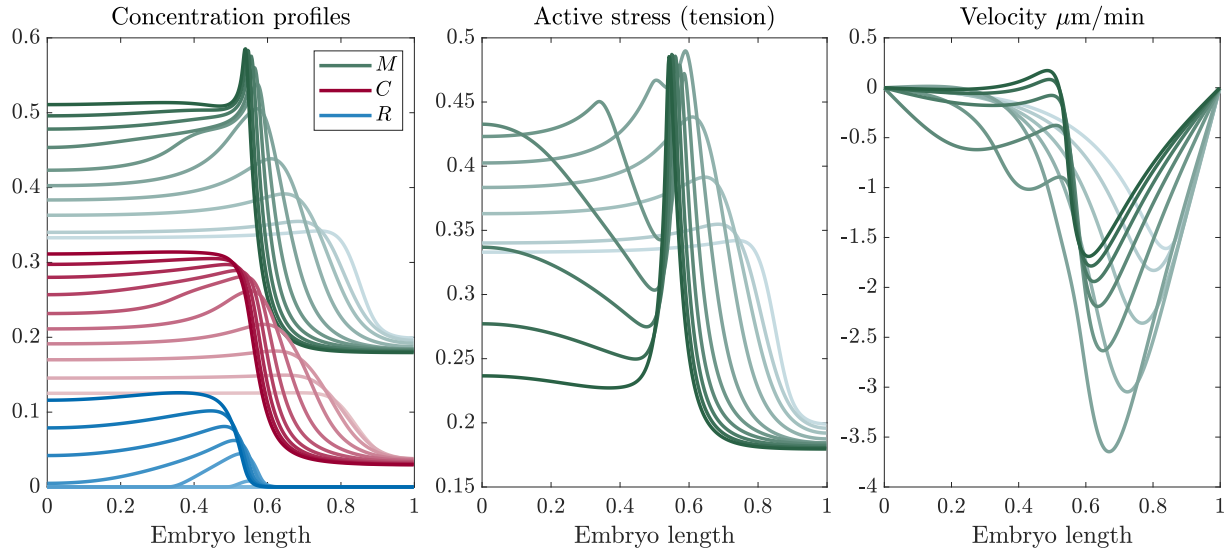

(a) Increased friction ($r_{\mathrm{R}\gamma} = 100$)

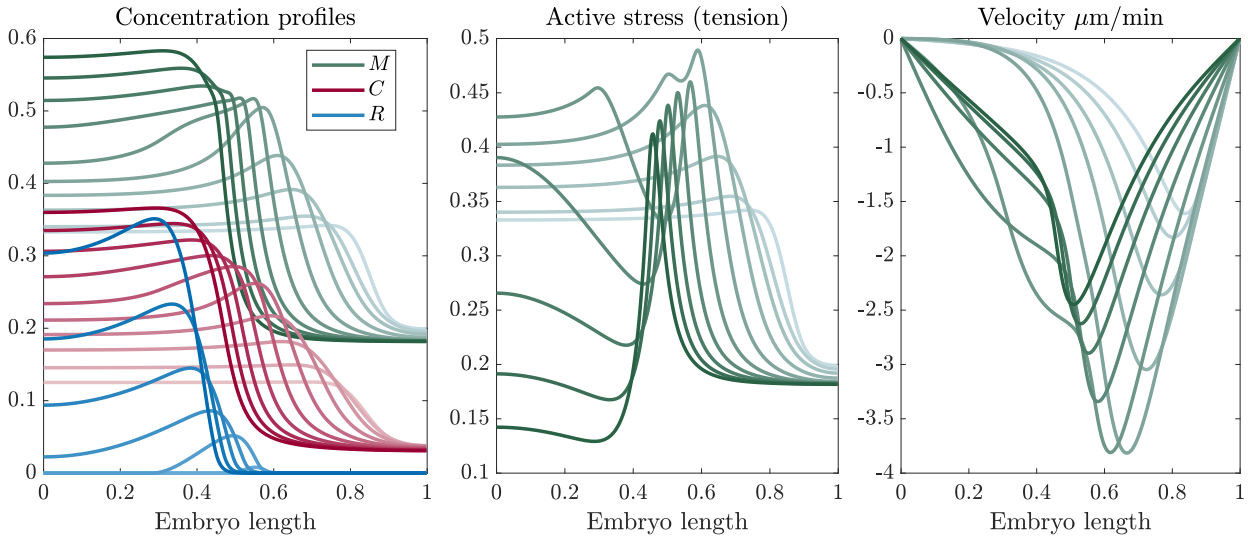

(b) Increased viscosity ($r_{\mathrm{R}\eta} = 20$)

Figure 10: Dynamics of rescue when branched actin has *severe* effects on the response to stress. In (a) viscosity is constant and friction increases according to $\gamma(R) = 1 + r_{\mathrm{R}\gamma}R$, while in (b) friction is constant and viscosity increases according to $\eta(R) = 1 + r_{\mathrm{R}\eta}R$ (note the linear velocity gradient where branched actin is enriched). The left panel shows the concentration profile of myosin (M, green), CDC-42 (C, red), and branched actin (R, blue) over time. The middle panel shows the active stress (tension), normalized by σ_0, and the right panel shows the velocity in units of μm/min. Each panel has a series of ten lines which show the profile at $t = 1, 2, \ldots 10$ min, with darker lines showing later times.

The main distinction between the two models happens when we further increase the dependence of friction/viscosity on branched actin. Suppose, for example that friction is ten times higher on the anterior (with branched actin) than in the posterior (without branched actin). Fig. 10(a) shows that this helps the model with increased friction draw closer to the data. We reproduce the sharp drop in velocity when the boundary stalls, and the reduced flows in the anterior preserve the myosin peak for longer (although eventually the peak will disappear because of the weaker velocity). The changes due to friction almost entirely kill the flow in the anterior.

We contrast this with the case where the *viscosity* is five times larger on the anterior (with brached actin) than in the posterior, which is shown in Fig. 10(b). Because of the large viscous resistance at the anterior, the rate of strain ($\partial_x v$) has to be constant there. At the anterior cap, the flow is in the negative direction (towards the anterior), and so in high viscosity all that can result is a linear profile moving towards zero at the anterior pole. Put another way, the viscous resistance prevents the velocity profile from rapidly (in space) responding to changes in contractility, and instead of a sharp transition to zero velocity we get a slow transition. The result of this, as shown in Fig. 10 is a boundary which never stops contracting.

5 Discussion

References

[1] Tom Bland, Nisha Hirani, David Briggs, Riccardo Rossetto, KangBo Ng, Neil Q McDonald, David Zwicker, and Nathan W Goehring. Optimized dimerization of the par-2 ring domain drives cooperative and selective membrane recruitment for robust feedback-driven cell polarization. *bioRxiv*, pages 2023–08, 2023.

[2] Justin S Bois, Frank Jülicher, and Stephan W Grill. Pattern formation in active fluids. *Biophysical Journal*, 100(3):445a, 2011.

[3] Agathe Chaigne, Clément Campillo, Nir S Gov, Raphaël Voituriez, C Sykes, Marie-Hélène Verlhac, and Marie-Emilie Terret. A narrow window of cortical tension guides asymmetric spindle positioning in the mouse oocyte. *Nature communications*, 6(1):6027, 2015.

[4] Rebecca J Cheeks, Julie C Canman, Willow N Gabriel, Nicole Meyer, Susan Strome, and Bob Goldstein. C. elegans par proteins function by mobilizing and stabilizing asymmetrically localized protein complexes. *Current Biology*, 14(10):851–862, 2004.

[5] Adrian A Cuenca, Aaron Schetter, Donato Aceto, Kenneth Kemphues, and Geraldine Seydoux. Polarization of the c. elegans zygote proceeds via distinct establishment and maintenance phases. 2003.

[6] Evan B Dewey, Danielle T Taylor, and Christopher A Johnston. Cell fate decision making through oriented cell division. *Journal of developmental biology*, 3(4):129–157, 2015.

[7] Wan Jun Gan and Fumio Motegi. Mechanochemical control of symmetry breaking in the caenorhabditis elegans zygote. *Frontiers in Cell and Developmental Biology*, 8:619869, 2021.

[8] Nathan W Goehring, Philipp Khuc Trong, Justin S Bois, Debanjan Chowdhury, Ernesto M Nicola, Anthony A Hyman, and Stephan W Grill. Polarization of par proteins by advective triggering of a pattern-forming system. *Science*, 334(6059):1137–1141, 2011.

[9] Bob Goldstein and Ian G Macara. The par proteins: fundamental players in animal cell polarization. *Developmental cell*, 13(5):609–622, 2007.

[10] Pierre Gönczy and Lesilee S Rose. Asymmetric cell division and axis formation in the embryo. *WormBook*, page 1, 2005.

[11] Peter Gross, K Vijay Kumar, Nathan W Goehring, Justin S Bois, Carsten Hoege, Frank Jülicher, and Stephan W Grill. Guiding self-organized pattern formation in cell polarity establishment. *Nature physics*, 15(3):293–300, 2019.

[12] Niv Ierushalmi and Kinneret Keren. Cytoskeletal symmetry breaking in animal cells. *Current Opinion in Cell Biology*, 72:91–99, 2021.

[13] Rukshala Illukkumbura, Nisha Hirani, Joana Borrego-Pinto, Tom Bland, KangBo Ng, Lars Hubatsch, Jessica McQuade, Robert G Endres, and Nathan W Goehring. Design principles for selective polarization of par proteins by cortical flows. *Journal of Cell Biology*, 222(8), 2023.

[14] Charles F Lang, Alexander Anneken, and Edwin Munro. Oligomerization and feedback on membrane recruitment stabilize par-3 asymmetries in c. elegans zygotes. *bioRxiv*, pages 2023–08, 2023.

[15] Charles F Lang and Edwin Munro. The par proteins: from molecular circuits to dynamic self-stabilizing cell polarity. *Development*, 144(19):3405–3416, 2017.

[16] Rong Li and Bruce Bowerman. Symmetry breaking in biology. *Cold Spring Harbor perspectives in biology*, 2(3):a003475, 2010.

[17] Jean-Léon Maître, Hervé Turlier, Rukshala Illukkumbura, Björn Eismann, Ritsuya Niwayama, François Nédélec, and Takashi Hiiragi. Asymmetric division of contractile domains couples cell positioning and fate specification. *Nature*, 536(7616):344–348, 2016.

[18] Mirjam Mayer, Martin Depken, Justin S Bois, Frank Jülicher, and Stephan W Grill. Anisotropies in cortical tension reveal the physical basis of polarizing cortical flows. *Nature*, 467(7315):617–621, 2010.

[19] Ani Michaud, Marcin Leda, Zachary T Swider, Songeun Kim, Jiaye He, Jennifer Landino, Jenna R Valley, Jan Huisken, Andrew B Goryachev, George von Dassow, et al. A versatile cortical pattern-forming circuit based on rho, f-actin, ect2, and rga-3/4. *Journal of Cell Biology*, 221(8):e202203017, 2022.

[20] Jonathan B Michaux, François B Robin, William M McFadden, and Edwin M Munro. Excitable rhoa dynamics drive pulsed contractions in the early c. elegans embryo. *Journal of Cell Biology*, 217(12):4230–4252, 2018.

[21] Edwin Munro, Jeremy Nance, and James R Priess. Cortical flows powered by asymmetrical contraction transport par proteins to establish and maintain anterior-posterior polarity in the early c. elegans embryo. *Developmental cell*, 7(3):413–424, 2004.

[22] Camelia G Muresan, Zachary Gao Sun, Vikrant Yadav, A Pasha Tabatabai, Laura Lanier, June Hyung Kim, Taeyoon Kim, and Michael P Murrell. F-actin architecture determines constraints on myosin thick filament motion. *Nature communications*, 13(1):7008, 2022.

[23] Masatoshi Nishikawa, Sundar Ram Naganathan, Frank Jülicher, and Stephan W Grill. Controlling contractile instabilities in the actomyosin cortex. *Elife*, 6:e19595, 2017.

[24] Dae Hwi Park and Lesilee S Rose. Dynamic localization of lin-5 and gpr-1/2 to cortical force generation domains during spindle positioning. *Developmental biology*, 315(1):42–54, 2008.

[25] Anne Sailer, Alexander Anneken, Younan Li, Sam Lee, and Edwin Munro. Dynamic opposition of clustered proteins stabilizes cortical polarity in the c. elegans zygote. *Developmental cell*, 35(1):131–142, 2015.

[26] Stephanie Schonegg, Alexandru T Constantinescu, Carsten Hoege, and Anthony A Hyman. The rho gtpase-activating proteins rga-3 and rga-4 are required to set the initial size of par domains in caenorhabditis elegans one-cell embryos. *Proceedings of the National Academy of Sciences*, 104(38):14976–14981, 2007.

[27] Stephanie Schonegg and Anthony A Hyman. Cdc-42 and rho-1 coordinate acto-myosin contractility and par protein localization during polarity establishment in c. elegans embryos. 2006.

[28] Yu Chung Tse, Michael Werner, Katrina M Longhini, Jean-Claude Labbe, Bob Goldstein, and Michael Glotzer. Rhoa activation during polarization and cytokinesis of the early caenorhabditis elegans embryo is differentially dependent on nop-1 and cyk-4. *Molecular biology of the cell*, 23(20):4020–4031, 2012.

[29] Meng-Fu Bryan Tsou, Adam Hayashi, Leah R DeBella, Garth McGrath, and Lesilee S Rose. Let-99 determines spindle position and is asymmetrically enriched in response to par polarity cues in c. elegans embryos. 2002.

[30] Qing Yang, Xiao-Feng Zhang, Thomas D Pollard, and Paul Forscher. Arp2/3 complex–dependent actin networks constrain myosin ii function in driving retrograde actin flow. *Journal of Cell Biology*, 197(7):939–956, 2012.

[31] Seth Zonies, Fumio Motegi, Yingsong Hao, and Geraldine Seydoux. Symmetry breaking and polarization of the c. elegans zygote by the polarity protein par-2. *Development*, 137(10):1669–1677, 2010.